



Numerical Analysis of High Aspect Ratio Flexible Wings in Flapping Motion

A. Shahzad^{†1}, M. N. Mumtaz Qadri¹ and S. Ahmad²

¹Department of Aerospace Engineering, College of Aeronautical Engineering, National University of Sciences & Technology, Pakistan

²Department of Mechanical Engineering, The Hong Kong Polytechnic University, Hong Kong, China

[†]Corresponding Author Email: a.shahzad@cae.nust.edu.pk

(Received October 28, 2018; accepted April 8, 2019)

ABSTRACT

Wing geometry, kinematics and flexibility are the fundamental components which contribute towards the aerodynamics performance of micro aerial vehicles. This research focuses on determining the role of isotropic flexibility in the aerodynamic performance of high aspect ratio ($AR = 6.0$) wings with different shapes in hovering flight. Three shapes are chosen, defined by the radius of the first moment of wing area \bar{r}_1 , which are 0.43, 0.53 and 0.63, where low (resp. high) value of \bar{r}_1 corresponds to less (resp. more) spanwise area distribution towards the wingtip. The leading edges of flexible wings are modelled as rigid and the wings, therefore, predominantly deform in the chordwise direction. Flexible wings are categorized as flexible FX2 and more flexible MFX2 for brevity. The governing equations of fluid flow are solved using a sharp interface immersed boundary method, coupled with an in-house finite element structure solver for simulations of flexible wings. The results indicate that the rigid wings produce one lift peak per stroke during the mid-stroke and its magnitude increases with an increase in \bar{r}_1 due to strong leading-edge vortex. For flexible wings, the numbers of lift peaks per stroke and their timings during a flapping cycle depend on the deformation that affects the pitch angle and pitch rotation rate of the wings. The lift coefficient for a given shape decreases as flexibility increases because the pitch angle decreases during the mid-stroke. This decrease in lift coefficient with flexibility is pronounced for $\bar{r}_1 = 0.63$ wing (up to 66 % less lift as compared to rigid equivalent) due to pitch down rotation at the commencement of the stroke, resulting in vortical structures on the bottom surface of the wing. For more flexible wings at high AR considered in this study, a wing with low \bar{r}_1 ($= 0.43$) may be suitable for the wing design of micro-aerial vehicle, as in general, it has better aerodynamic performance (24.5 % more power economy and similar lift coefficient) than high \bar{r}_1 ($= 0.63$) wing.

Keywords: Flapping wings; Wing shape; Aspect ratio; Fluid-structure interaction; Micro aerial vehicle.

NOMENCLATURE

AR	aspect ratio	Re	Reynolds number
c	mean chord length	S	wing area
C_L	lift coefficient	U	reference velocity
C_{Pa}	power coefficient	U_{tip}	mean wingtip velocity
C_p	pressure coefficient	ν	poisson's ratio
E^*	non-dimensional young's modulus		
E	young's modulus	f_n	natural frequency
F_L	lift force	π_1	effective stiffness
f	flapping frequency	ρ^*	density ratio
h_s	wing thickness	ρ_f	fluid density
h^*	non-dimensional thickness	ρ_s	structure density
I	bending second moment of plate area	Φ	stroke amplitude
m^*	mass ratio	α	pitch angle
p	pressure	μ	dynamic viscosity
P_a	aerodynamic power	ϕ	stroke angle
R	wing length		
\bar{r}_1	the radius of the first moment of wing area		

1. INTRODUCTION

Inspired by the flight of insects and birds, there has always been a human desire to fly. Building on the concepts of George Cayley, a giant leap in this direction was taken in 1903 when Orville Wright made history by flying a distance of 120 *ft* in an erratic flight of 12 *seconds* (Anderson, 1989). Modern jets flying at high speeds and commercial planes carrying tonnes of load over long distances, both equipped with sophisticated technologies, provide enough evidence that rapid progress in the field of aerospace has been made since the first flight. However, emulating the enviable flight characteristics of small-sized natural fliers such as hovering and high manoeuvrability remains a farfetched reality. During the First World War, the development of pilotless airplanes called unmanned aerial vehicles (UAVs) added a new dimension to the concept of flying. In 1996, a special class of UAV called the micro aerial vehicle (MAV) came into the limelight, with a wingspan less than 15 *cm* and mass up to 100g (McMichael and Francis, 1997) as defined by US Defense Advanced Research Projects Agency (McMichael and Francis, 1997). Since then, different applications of MAVs in the military and other fields such as sports and agriculture have been under consideration.

The structure of insect wings is markedly different from conventional airplanes. A wing of an insect is comparatively stiffer at the root and leading edge (LE) than the rest of the wing (Combes and Daniel, 2003a, Combes and Daniel, 2003b), and there is a network of veins with versatile patterns running along the span (Combes, 2010). Unlike birds, the motion in insects is imparted to the root of the wing via the flight muscles, while the rest of the wing deforms passively during flight. In the past, flapping flight studies have generally been conducted on rigid wings (Dickinson *et al.*, 1999; Birch and Dickinson, 2001; Birch and Dickinson, 2003; Luo and Sun, 2005; Harbig *et al.*, 2013; Harbig *et al.*, 2014).

The simplest way to model wing flexibility is to use an isotropic material as done in our previous works (Shahzad, 2017; Shahzad *et al.*, 2018a). Likewise, Aono *et al.* (2010) performed a numerical study on Zimmerman wings in one DoF flapping motion with isotropic flexibility defined by $\pi_1 = 1.4 \times 10^3$ and 35.5×10^3 . They found that the least stiff wing produces thrust due to induced positive pitch angle and gives more lift due to tip deformation, which results in higher wingtip velocity attributable to strong vortical structures on the wing surface. Zhao *et al.* (2010) designed isotropic flexible wings with a rigid LE to perform experiments at a fixed angle of attack (AoA) for a stroke amplitude of 180° . They found that the lift and drag decrease with the increase in flexibility for low angles of attack (up to 50°). However, at high angles of attack, flexible wings attain a lift plateau before producing more lift than the rigid wing. As compared to the rigid wing with maximum lift at an angle of attack of 45° , the maximum lift of flexible wings varied with flexibility. The lift to drag ratio was insensitive to

angles of attack between 20° and 60° . Zheng *et al.* (2015) modelled three sets of flexible wings by varying the thickness. They observed that a flexible wing designed with a thickness of 1 mm generated 19.4 % more lift than a rigid wing, however, further increase in flexibility was unfavourable to lift production. For just decreasing the thickness by 0.5 mm, a 43.7 % decrease in lift was recorded. Kang *et al.* (2011) performed numerical computations to study the effects of ρ^* and π_1 on deformation and lift generation of Zimmerman wing planform hovering at Re of 1.5×10^3 . They observed that a balance between ρ^* and π_1 has a significant effect on deformation characteristics and lift production. This research as well as other works indicate that the wing flexibility, if employed appropriately in combination with given geometric and kinematic parameters, may be beneficial to the aerodynamic performance of MAV.

Shahzad *et al.* (2018a) carried out numerical simulations on rigid and flexible wings with three values of \bar{r}_1 and four values of AR to measure the aerodynamic performance in hovering flight. At mass ratio $m^* = 4.0$, flexible (FX) and more flexible (MFX) wings were defined by $\pi_1 = 14$ and 6.12, respectively for all shapes and ARs. For high AR wings (AR = 6.0), it was found that deformation resulted in a decrease in C_L and an increase in power economy PE due to smaller α during mid-stroke than rigid wings. For example, 3.5 % less C_L and 12.3 % more PE of $\bar{r}_1 = 0.63$ MFX wing. At AR = 6.0, there was limited deformation at $\pi_1 = 14$ and 6.12 considered in the study, and the frequency ratio (f/f_n) did not exceed 0.14 for any shape. The frequency ratio of insect wings can be even higher, for example, 0.3 for hawkmoth and about 0.45 for cicada. As wings with frequency ratios higher than 0.14 do exist in nature, for MAV applications, there may be a potential benefit of using even higher flexible wings than those considered in our previous work at AR = 6.0. Hence, there is a need to perform further fluid-structure interaction simulations of different wings with AR = 6.0 by using π_1 even lower than 6.12, which was considered in our previous work (Shahzad *et al.*, 2018a).

Inspired by our findings as mentioned in the preceding paragraph, in this research, numerical simulations are carried out for wings with different radius of the first moment of wing area ($\bar{r}_1 = 0.43, 0.53$ and 0.63), and $\pi_1 = 1.32$ and 0.58 for flexible and more flexible wings respectively. The aim is to investigate the role of flexibility in the aerodynamic performance of a flapping wing for MAV application. The flexible and more flexible wings, here, are symbolized as FX2 and MFX2 respectively to distinguish it from our previous work. The simulations are carried out at Re of 400, based on U_{tip} as a reference velocity and c as a reference length, representative of insects and bio-inspired MAVs (Shyy *et al.*, 2013). The Re of insects can be as low as the order $O(10)$ to as high as the order $O(10^3)$. For example, Re is about 10, 400 and 6000 for thrips, hoverfly and dragonfly, respectively.

2. WING SHAPES, KINEMATICS AND MATERIAL PROPERTIES

There is extensive variation in wing morphological parameters found in nature, and the details of these parameters for different insect wings have been recorded in the past (Sotavalta, 1952, Weis-Fogh, 1973, Ellington, 1984). Ellington (1984) observed that most wing shapes of insects could be approximated by the radius of the first moment of the wing area (\bar{r}_1) that defines the distribution of the wing area along the span. We have used $\bar{r}_1 = 0.43, 0.53$ and 0.63 to define wing shapes (see Fig. 1(a)), and in line with our research objectives mentioned in the previous section, only $AR = 6.0$ is considered in this work. As in our previous studies (Shahzad *et al.*, 2018a; Shahzad *et al.*, 2018b), two degrees of freedom (DoF) kinematics have been used, and it is defined by the sinusoidal function for stroke angle ϕ and truncated Fourier series for pitch angle α (both in degrees) as follows:

$$\begin{aligned} \phi &= \phi_0 \sin(\alpha t - 1.579), & (1) \\ \alpha &= 180 - (89.1 + 16\cos(\alpha t) + 46.2\cos(2\alpha t) & (2) \\ &- 0.06\cos(2\alpha t) - 0.1\sin(2\alpha t) + 5.04\cos(3\alpha t) \\ &+ 0.40\sin(3\alpha t) - 0.10\cos(4\alpha t) - 0.14\sin(4\alpha t) \\ &- 0.44\cos(5\alpha t) - 0.53\sin(5\alpha t)) \end{aligned}$$

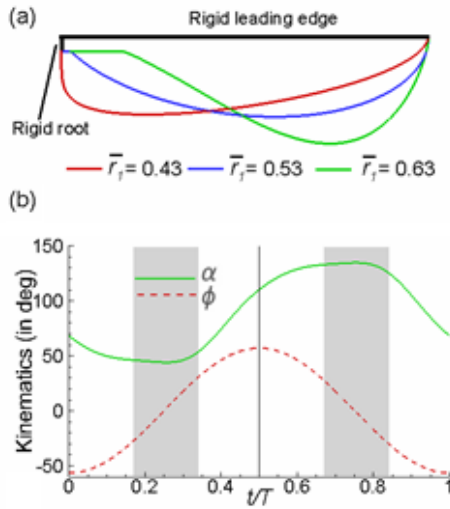


Fig. 1. (a) Wing shapes defined by \bar{r}_1 and (b) time courses of stroke and pitch angles in degrees. Grey shaded areas in (b) represent mid-strokes.

The time courses of ϕ and α are given in Fig. 1(b). The stroke refers to azimuth rotation in a horizontal plane. The wing pitches about leading edge LE and the pitch angle is defined as the angle α between a horizontal axis and the line joining LE to the trailing edge at the mid-span. The readers are referred to Shahzad *et al.* (2018a) for further details about wing shapes and kinematics.

As shown in Fig. 1(a), the leading edge is modelled as rigid, and the root up to $0.25c$ from the leading edge is also modelled as rigid. Rest of the wing is a membrane modelled with homogenous and isotropic

Kirchhoff triangular plate elements. Enough number of elements were chosen to keep the wing deformation properties unchanged with a further increase in the number of elements. We have assumed Poisson's ratio as 0.3. Flexibility is incorporated by changing Young's modulus E^* of plate elements for FX2 and MFX2 wings, which in turn leads to a change in effective stiffness π_1 . The material properties of wings are given in Table 1, and the frequency ratios of wings calculated from the modal analysis are given in Table 2. It is pertinent to mention that the hawkmoth has a frequency ratio of around 0.3 (San Ha *et al.*, 2013) and the flexibility parameters in Table 1 adequately cover a wide range of frequency ratios including 0.3, as shown in Table 2.

Table 1 Flexibility parameters of wings

Material properties	FX2	MFX2
E^*	1.80×10^9	7.91×10^8
h^*	2.0×10^{-3}	2.0×10^{-3}
I	6.67×10^{-10}	6.67×10^{-10}
ρ^*	2×10^3	2×10^3
π_1	1.32	0.58

Table 2 Frequency ratios of wings with $f = 20$ Hz

Wing shapes	Flexibility	f_n (in Hz)	f/f_n
$\bar{r}_1 = 0.43$	FX2	111.19	0.18
$\bar{r}_1 = 0.53$		107.55	0.19
$\bar{r}_1 = 0.63$		66.93	0.30
$\bar{r}_1 = 0.43$	MFX2	73.69	0.27
$\bar{r}_1 = 0.53$		71.28	0.28
$\bar{r}_1 = 0.63$		44.36	0.45

3. COMPUTATIONAL METHODS

Following continuity and Navier-Stokes equations are solved using an inhouse fluid solver developed by Mittal *et al.* (2008) and based on a 2^{nd} order sharp interface immersed boundary method:

$$\frac{\partial v_i}{\partial x_i} = 0, \quad (3)$$

$$\rho_f \frac{\partial v_i}{\partial t} + \rho_f \frac{\partial v_j v_i}{\partial x_j} = -\frac{\partial p}{\partial x_i} + \rho_f \nu \frac{\partial}{\partial x_j} \left(\frac{\partial v_i}{\partial x_j} \right), \quad (4)$$

where $i = 1, 2, 3$ and $j = 1, 2, 3$ in subscripts, \mathbf{v} is the velocity, t is the time, and ν is the kinematic viscosity. The flow is assumed as viscous and incompressible. Reynolds number of 400 used in this study is low enough that we can fairly assume laminar flow for computations. The structural dynamics is governed by the following equation (Tian *et al.*, 2014a):

$$\rho_s \frac{d^2 u_i}{dt^2} + \eta_d \frac{du_i}{dt} = \frac{\partial \sigma_{ij}}{\partial x_j} + \rho_s b_i, \quad (5)$$

where \mathbf{u} is the displacement, η_d is the damping coefficient, σ_{ij} is the Cauchy stress tensor, \mathbf{b}_i is the body force, and (d/dt) is the Lagrangian time derivative. The structure solver, NONSTAD (non-linear analysis of statics and dynamics), is a finite element analysis tool of solid mechanics developed by James F. Doyle (2001, 2008) and it is suitable for bio-mimetic structures as it is specifically designed for the analysis of thin-walled structures comprising membranes, plates, shells, and frames. The details of both fluid and structure solvers can be found in Dai (2013) and Tian *et al.* (2014a). In FSI solver, a modular iterative partitioned approach is used, and both solvers are strongly coupled through no-slip, no-penetration and traction boundary conditions.

A computational domain stretching about $25c$ in all directions is divided into sub-domains; inner and outer. The domain consists of a non-uniform cartesian mesh as shown in Fig. 2. While the mesh density is varied in the inner domain, 50 nodes are used in each direction on the outer domain in grid independence studies to obtain an appropriate mesh

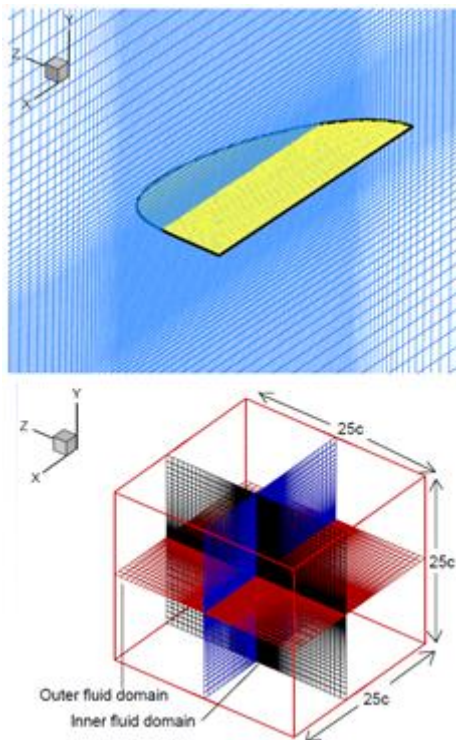


Fig. 2. (a) Cartesian mesh around the wing, and (b) A cut-out of fluid computational domain comprising a fine inner fluid domain and relatively coarse outer fluid domain. The domain extents are $25c$ in each direction (that is, X, Y, and Z directions). (Shahzad *et al.*, 2018a).

size for further simulations. Likewise, time independence tests have also been carried out to adequately capture the flow structures. For details about grid and time independence tests, readers are

referred to Shahzad *et al.* (2018a). As in our previous work (Shahzad *et al.*, 2018a), a mesh of 0.14 million is employed in the inner fluid domain. The results of the fifth flapping cycle are used for postprocessing, with each cycle completed in 2000 timesteps. In addition, the validations of fluid solver and FSI solver against known experimental results have been extensively done in our previous works (Shahzad *et al.*, 2014; Shahzad *et al.*, 2016a; Shahzad *et al.*, 2016b; Shahzad, 2017; Shahzad *et al.*, 2018a; Shahzad *et al.*, 2018b), and thus, are not presented here for brevity.

4. RESULTS AND DISCUSSION

Each computation took 180 hrs/flapping cycle on 8 cores of Intel Xeon E5-2680 processors and 64 GB of memory. A total of five flapping cycles were simulated and the results of the last cycle were used for post-processing, as the time courses of C_L and C_{Pa} did not vary more than 1.5% between 4th and 5th cycle.

4.1 Time Courses of C_L and C_{Pa} of RG, FX2 and MFX2 Wings of Different Shapes

The time courses of C_L and C_{Pa} for rigid (RG), FX2 and MFX2 wings are compared in Fig. 3. Both strokes during the flapping cycle are similar, hence only the first stroke ($t/T = 0.0 - 0.5$) will be discussed.

All RG wings produce one C_L peak and one C_{Pa} peak per stroke during the mid-stroke (the grey shaded portion between $t/T = 0.17$ and 0.34 in Fig. 3(a) and Fig. 3(c) and both peaks increase with an increase in \bar{r}_1 . The FX2 wings produce considerably less C_L and also consume less C_{Pa} during the mid-stroke as compared to RG wing, especially for $\bar{r}_1 = 0.63$ wing in which C_L drops by 34.3 % at $t/T = 0.212$, and C_{Pa} drops by 52.4 % at $t/T = 0.34$ with the introduction of flexibility. In contrast with a single peak in RG wing of $\bar{r}_1 = 0.63$, the flexible equivalent (FX2) produces two C_L and two C_{Pa} peaks per stroke (see Fig. 3(a) and Fig. 3(c)). The values of C_L in Fig. 3(b) suggest that the more flexible (MFX2) wings of $\bar{r}_1 = 0.43$ and 0.53 show similar trends as those of corresponding RG and FX2 wings in Fig. 3(a). However, the MFX2 wing of $\bar{r}_1 = 0.63$ generates a negative lift peak at $t/T = 0.06$ and one positive peak at $t/T = 0.22$ accompanied by a C_L plateau after the mid-stroke, and this contrasts with a solitary C_L peak in RG equivalent wing. The C_{Pa} consumed by each wing decreases further as the wings are made more flexible (see Fig. 3(c) and Fig. 3(d)).

4.2 Pitch Angles, Pitch Rotation Rates, and Flow Features of RG, FX2 and MFX2 Wings

The reasons for trends in C_L and C_{Pa} of RG, FX2 and MFX2 wings observed in Fig. 3 have been explained by plotting the variations of pitch angle and pitch rotation rates at the mid-span in Fig. 4 accompanied by details of flow features using iso-Q surfaces and surface pressure coefficients at selected time instants. The iso-Q surfaces are based on the vortex identification criterion of Hunt *et al.* (1988) which

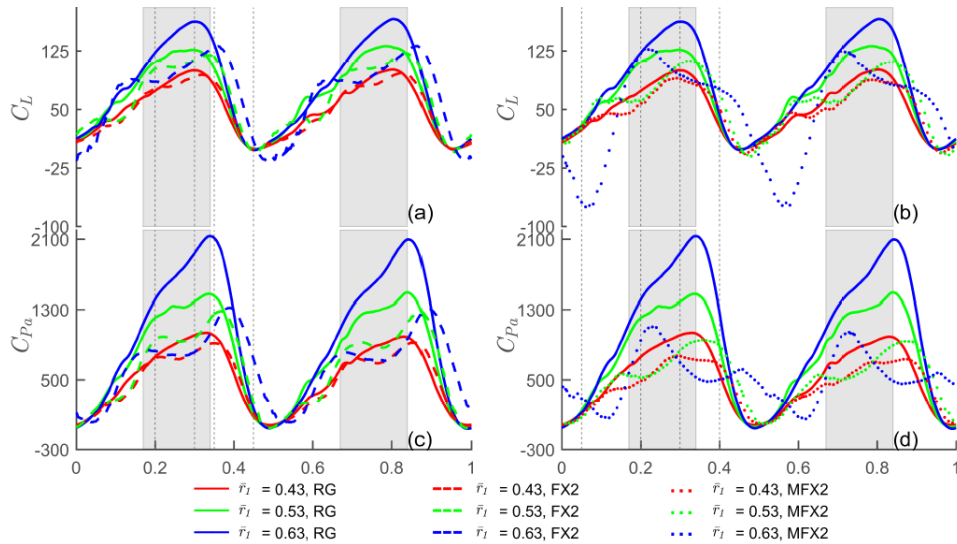


Fig. 3. Comparison of time courses of coefficients of lift (C_L) and aerodynamic power (C_{Pa}) of rigid (RG), flexible (FX2) and more flexible (MFX2) wings in a flapping cycle. The grey shaded portion refers to a region of mid-stroke, where pitch angle does not vary appreciably.

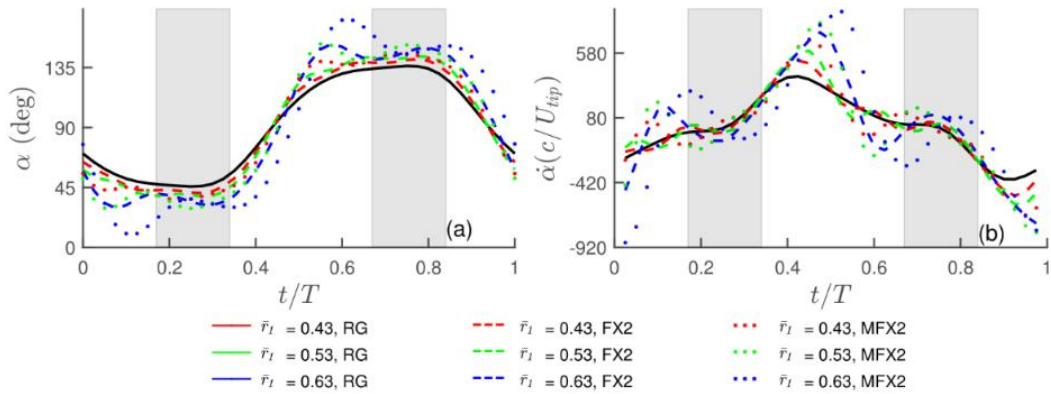


Fig. 4. Comparison of time courses of pitch angles and pitch rotation rates of rigid (RG), flexible (FX2) and more flexible (MFX2) wings in a flapping cycle.

separates fluid motion into strain and shear rates, and rigid-body-like rotation rates. For brevity, only the flow features of $\bar{r}_1 = 0.43$ and 0.63 wings are compared.

4.2.1 RG vs. FX2 Wings

For FX2 with $\bar{r}_1 = 0.43$, at $t/T = 0.2$ and 0.3 , α is approximately 3° less than RG wing (Fig. 4(a)), and the vortical structures (Fig. 5 (a and b) at $t/T = 0.2$ and Fig. 5 (e and f) at $t/T = 0.3$) and surface pressure distribution on the top surface (Fig. 6 (a and b) at $t/T = 0.2$ and Fig. 6 (e and f) at $t/T = 0.3$) are similar for RG and FX2 wings. As a result, both RG and FX2 wings produce similar lift.

For $\bar{r}_1 = 0.63$ FX2, during the mid-stroke at $t/T = 0.2$ and 0.3 , there is a continuous pitch down rotation and α remains less than RG wing. Hence, the Iso-Q surfaces in Fig. 5 (c, d, g and h) shows a stronger LEV on RG wings than FX2 wings. Similarly, a large negative pressure region on the upper surface of the RG wing leads to more lift than the FX2 wing (see

Fig 6 (c, d, g and h)).

At $t/T = 0.35$, the pitch angles of RG wings are 57.4° , and $\bar{r}_1 = 0.43$ FX2 and $\bar{r}_1 = 0.63$ FX2 are 51.7° and 41.6° respectively, as the wings pitch up after the mid-stroke. At this point, the LEVs are attached to the wing (see Fig. 5 (i, j, k and l)) and RG wings have greater strength than FX2 wings in terms of suction pressures as presented in Fig. 6. (i, j, k and l).

However, RG wings of both shapes do not produce significantly higher C_L than FX2 wings. This is due to the resultant force contributing more to horizontal component (drag) than to vertical component (lift) due to high pitch angles ($\alpha > 45^\circ$) of the wing. Consequently, the C_{Pa} peak is recorded by all RG wings at this instant.

At $t/T = 0.45$, the pitch angles of all wings are close to 90° and relatively weaker LEVs are mostly confined to the region of low flapping velocities close to the wing root as illustrated in Figs. 5 and 6 (m, n, o and p). The wings do not produce lift at this stage.

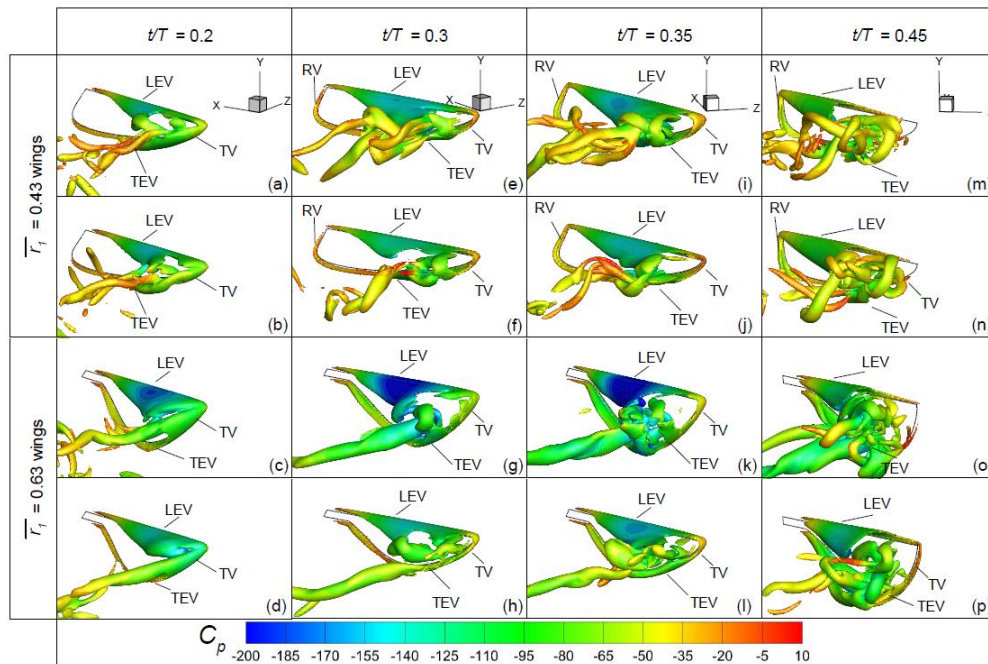


Fig. 5. Flow structures ($Q = 300$) on rigid (RG) and flexible (FX2) wings at different time instants in a flapping cycle.

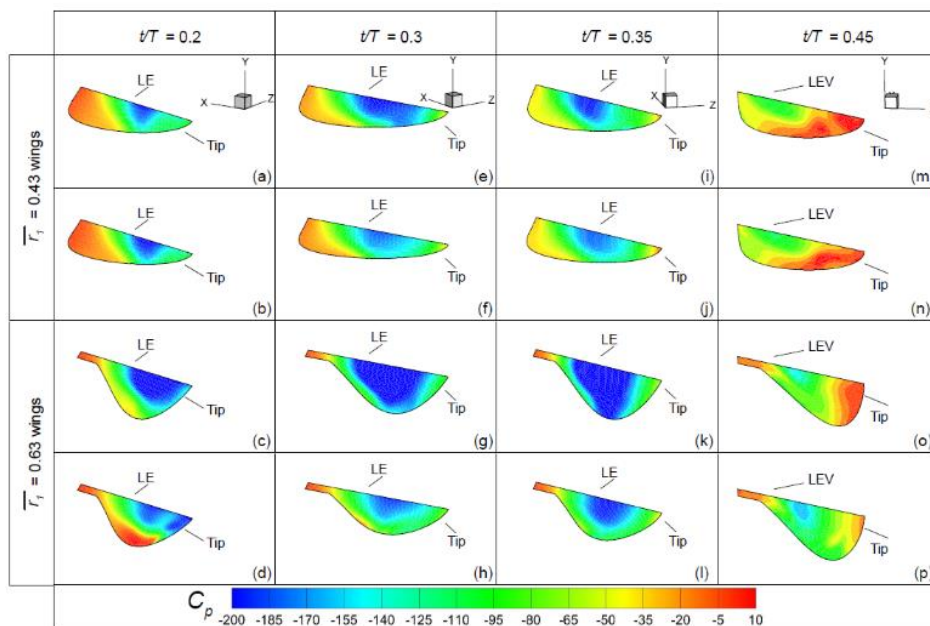


Fig. 6. Pressure coefficient on the surface of rigid (RG) and flexible (FX2) wings at different time instants in a flapping cycle.

4.2.2 RG vs. MFX2 Wings

At $t/T = 0.05$, both RG and MFX2 wings of $\bar{r}_1 = 0.43$ and RG wing of $\bar{r}_1 = 0.63$ give small positive C_L as the wing has just commenced a stroke. The vortical structures are mainly confined to a region close to the tip and, therefore, suction pressures are also high (see Figs. 7 and 8 (a, b and c)). On the contrary, $\bar{r}_1 = 0.63$ MFX2 records a large negative C_L at this point because α of the wing equals 33° and decreases

further (see Fig. 4(a)) as the wing continues to pitch down. Figure 7 shows the pressure distribution on the wing's top surface, which are very low since the vortices are present on the wing's lower surface at this instant.

At $t/T = 0.2$ and 0.3 , the $\bar{r}_1 = 0.43$ RG wing produces slightly more C_L than MFX2 wing as confirmed by higher suction pressures in Fig. 8(e and i). At $t/T = 0.2$, although α of $\bar{r}_1 = 0.63$ MFX2 wing is 35 %

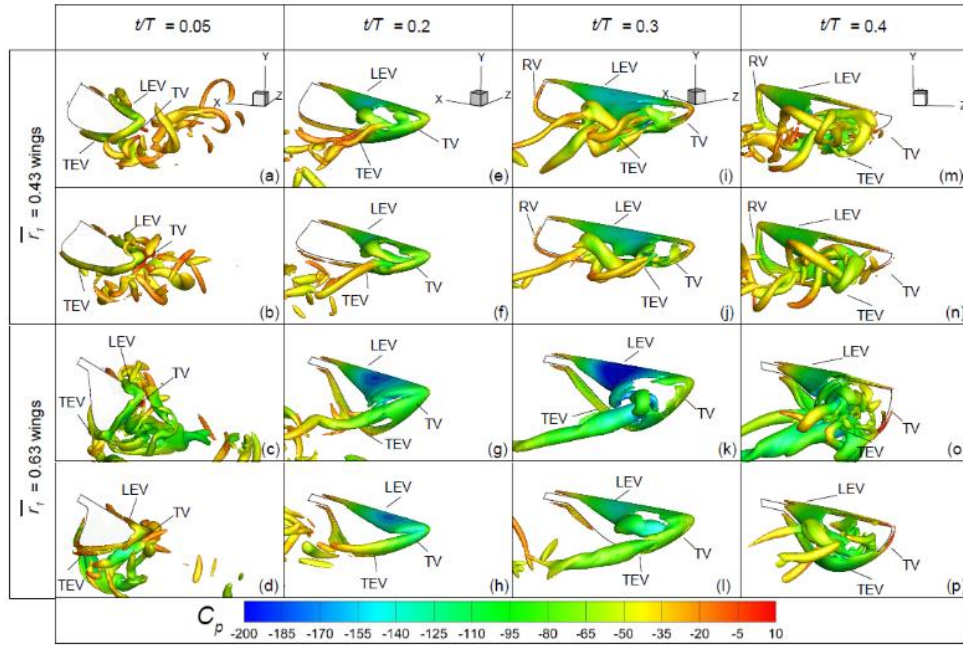


Fig. 7. Flow structures ($Q = 300$) on rigid (RG) and more flexible (MFX2) wings at different time instants in a flapping cycle.

smaller than RG equivalent in Fig. 4(a), the MFX2 wing is in pitch-up rotation mode and it has significantly higher pitch rotation rate in Fig. 4(b). Therefore, despite having a smaller value of α , $\bar{r}_1 = 0.63$ MFX2 wing is still able to produce a comparable C_L at $t/T = 0.2$. In contrast, the C_L of $\bar{r}_1 = 0.63$ MFX2 drops significantly below the RG equivalent because the MFX2 with 32 % smaller α than RG equivalent in Fig. 4(a) starts pitch down rotation after approximately $t/T = 0.25$ resulting into relatively weaker LEV in Fig. 7(l) and low suction pressures in Fig. 8(l).

At $t/T = 0.4$, α of RG wing is approaching 90° ($\alpha = 75^\circ$) and the resultant force contributes more to the drag. At this point, the LEVs on the wings are confined to the region close to the root (see Figs. 7 and 8 (m, n, o and p)) and do not contribute significantly to lift production. However, the trailing edge of $\bar{r}_1 = 0.63$ MFX2 wing is shifted rearward due to chordwise deformation and there is presence of a trailing edge vortex resulting in high suction pressures in Fig. 8(p), which translate into relatively more lift in $\bar{r}_1 = 0.63$ MFX2 wing as compared to RG equivalent.

The above-mentioned flow details on flexible and more flexible wings in different phases of the flapping cycle clearly indicate that flexibility can have both favourable and adverse effect on lift production and aerodynamic power depending on the deformation characteristics.

4.3 Comparison of Mean Lift Coefficient and Aerodynamic Power Coefficient of RG, FX2 and MFX2 Wings

In this section we discuss the \bar{C}_L , calculated by averaging C_L over the third, fourth and fifth flapping

cycles and power economy (PE defined as \bar{C}_L/\bar{C}_{Pa}) of all wings. The impact of flexibility on hovering performance has been evaluated in Fig. 9 by plotting PE against \bar{C}_L . Irrespective of wing shape, flexibility has a negative effect on \bar{C}_L and a substantial decrease of up to 66 % in \bar{C}_L is registered for $\bar{r}_1 = 0.63$ MFX2 wing attributable to large values of negative C_L at the start of each stroke (see Fig. 3(b)) due to pitch down rotation. The PE of $\bar{r}_1 = 0.43$ and 0.53 wings, for both FX2 and MFX2 cases, increases with an increased flexibility. However, the MFX2 wing of $\bar{r}_1 = 0.63$ records 12.6 % less PE than the FX2 wing. This implies that, at high AR considered in this study, if it is desirable to introduce flexibility to enhance aerodynamic performance, low \bar{r}_1 ($= 0.43$) wing shape may be preferred, provided it meets the minimum lift requirement for hovering.

5. CONCLUSIONS

Fluid-structure interaction simulations were performed using an in-house solver to evaluate the influence of isotropic flexibility on the aerodynamic performance of high AR ($= 6.0$) wings with different shapes ($\bar{r}_1 = 0.43, 0.53$ and 0.63) and $m^* = 4.0$. For flexible wings, the leading edge is assumed rigid and the flexibility of rest of the wing is defined by effective stiffness of 1.32 for flexible (FX2) wings and 0.58 for more flexible (MFX2) wings. This study is an extension of our previous work in which $\pi_1 = 14$ and 6.12 were used for FX and MFX wings.

The FX2 wings produce less C_L and C_{Pa} during most of the mid-stroke, as α decreases due to flexibility. The lift production decreases more appreciably for

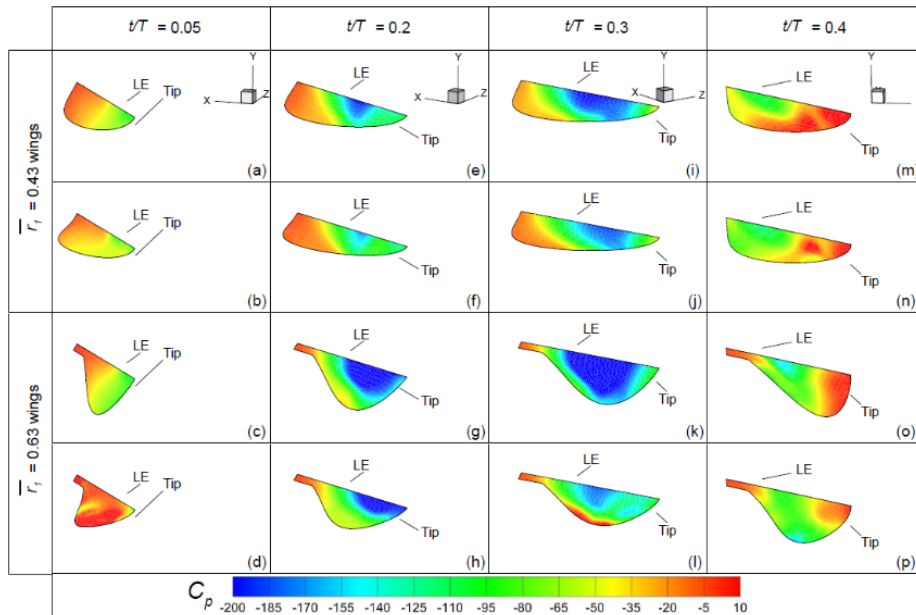


Fig. 8. Pressure coefficient on the surface of rigid (RG) and more flexible (MFX2) wings at different time instants in a flapping cycle.

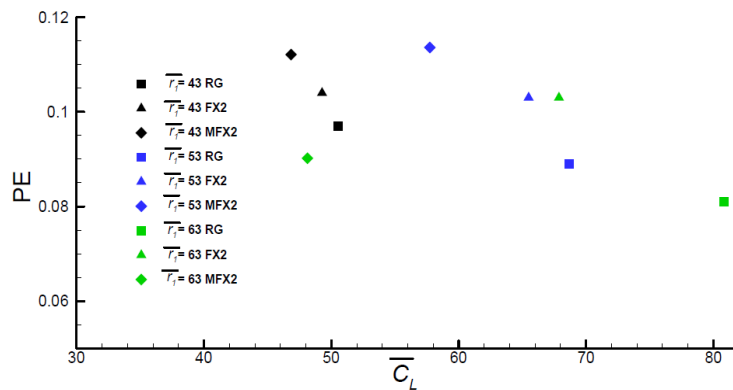


Fig. 9. Comparison of mean coefficient of lift and power economy of rigid (RG), flexible (FX2) and more flexible (MFX2) wings in a flapping cycle.

high $\bar{r}_1 (= 0.63)$ wing due to higher pitch down rotation translating into weaker LEV. The C_L and C_{Pa} of $\bar{r}_1 = 0.63$ FX2 wing reduces up to 34.3 % and 52.4 % at different instants during the mid-stroke.

As the flexibility is increased further, $\bar{r}_1 = 0.63$ MFX2 wing generates large negative C_L at the start of stroke because of small α and a continuous pitch-down rotation due to chordwise deformation.

In general, mean lift coefficient (\bar{C}_L) decreases by introducing flexibility, and it results in better power economy (PE) except for $\bar{r}_1 = 0.63$ MFX2 wing in which PE of MFX2 wing is 12.6 % less than FX2 wing.

If the wings are designed to be highly flexible like the MFX2 wings in this study, it is preferable to use low $\bar{r}_1 (= 0.43)$ wings as compared to high $\bar{r}_1 (= 0.63)$ wings since they can give better aerodynamic performance with higher PE and similar \bar{C}_L to an equivalent wing of $\bar{r}_1 = 0.63$. For instance, $\bar{r}_1 = 0.43$ MFX2 wing gives 24.5% more PE and 2.7 % less \bar{C}_L than $\bar{r}_1 = 0.63$ MFX2 wing.

ACKNOWLEDGEMENTS

The authors would like to acknowledge that the numerical simulations in this work were performed using high-performance workstations in the numerical analysis lab (NAL) at College of Aeronautical Engineering, National University of Sciences and Technology (NUST), Pakistan.

REFERENCES

- Anderson, J. (1989). *Introduction to Flight*, McGraw-Hill, New York, USA.
- Aono, H., S. K. Chimakurthi, C. E. Cesnik, H. Liu and Shyy (2010). A computational and experimental study of flexible flapping wing aerodynamics. *48th AIAA aerospace sciences meeting including the new horizons forum and aerospace exposition*, Orlando, Florida, AIAA 2010-554.

- Birch, J. M. and M. H. Dickinson (2001). Spanwise flow and the attachment of the leading-edge vortex on insect wings. *Nature* 412(6848),729-733.
- Birch, J. M. and M. H. Dickinson (2003). The influence of wing-wake interactions on the production of aerodynamic forces in flapping flight. *Journal of Experimental Biology* 206(13),2257-2272.
- Combes, S. and T. Daniel (2003b). Flexural stiffness in insect wings II. Spatial distribution and dynamic wing bending. *Journal of Experimental Biology* 206(17), 2989-2997.
- Combes, S. A. (2010). Materials, structure, and dynamics of insect wings as bioinspiration for MAVs. *Encyclopedia of Aerospace Engineering*.
- Combes, S. A. and T. L. Daniel (2003a). Flexural stiffness in insect wings I. Scaling and the influence of wing venation. *Journal of Experimental Biology* 206(17), 2979-2987.
- Dai, H. (2013). *Computational modeling of fluid-structure interaction in biological flying and swimming*, Vanderbilt University.
- Dickinson, M. H., F.-O. Lehmann and S. P. Sane (1999). Wing rotation and the aerodynamic basis of insect flight. *Science* 284(5422), 1954-1960.
- Doyle, J. (2008). *QED: static, dynamic, stability, and nonlinear analysis of solids and structures*, Software manual, version 4.60, ikayex software tools.
- Doyle, J. F. (2001). *Nonlinear analysis of thin-walled structures: statics, dynamics, and stability*, Springer-Verlag, New York, USA.
- Ellington, C. (1984). The aerodynamics of insect flight. II. Morphological parameters. *Philosophical Transactions of the Royal Society B* 305: 17-40.
- Harbig, R., J. Sheridan and M. Thompson (2013). Reynolds number and aspect ratio effects on the leading-edge vortex for rotating insect wing planforms. *Journal of Fluid Mechanics* 717, 166-192.
- Harbig, R., J. Sheridan and M. Thompson (2014). The role of advance ratio and aspect ratio in determining leading-edge vortex stability for flapping flight. *Journal of Fluid Mechanics* 751, 71-105.
- Hunt, J. C., A. Wray and P. Moin (1988). Eddies, streams, and convergence zones in turbulent flows. Center for Turbulence Research Report CTR-S88. USA, 193-208,
- Kang, C. K., H. Aono, C. E. Cesnik and W. Shyy (2011). Effects of flexibility on the aerodynamic performance of flapping wings. *Journal of Fluid Mechanics* 689, 32-74.
- Luo, G. and M. Sun (2005). The effects of corrugation and wing planform on the aerodynamic force production of sweeping model insect wings. *Acta Mechanica Sinica* 21(6), 531-541.
- McMichael, J. M. and M. S. Francis (1997). Micro air vehicles-toward a new dimension in flight. *DARPA document* 1-9.
- Mittal, R., H. Dong, M. Bozkurttas, F. Najjar, A. Vargas and A. Von Loebbecke (2008). A versatile sharp interface immersed boundary method for incompressible flows with complex boundaries. *Journal of computational physics* 227(10), 4825-4852.
- San Ha, N., Q. T. Truong, N. S. Goo and H. C. Park (2013). Relationship between wingbeat frequency and resonant frequency of the wing in insects. *Bioinspiration & biomimetics* 8(4), 1-14.
- Shahzad, A., F. B. Tian, J. Young and J. C. Lai (2018a). Effects of flexibility on the hovering performance of flapping wings with different shapes and aspect ratios. *Journal of Fluids and Structures* 81, 69-96.
- Shahzad, A., F. B. Tian, J. Young and J. C. Lai (2018b). Effects of hawkmoth-like flexibility on the aerodynamic performance of flapping wings with different shapes and aspect ratios. *Physics of Fluids*.
- Shahzad, A., F. B. Tian, J. Young and J. C. Lai (2016a). "Effects of wing shape, aspect ratio and deviation angle on aerodynamic performance of flapping wings in hover. *Physics of Fluids* 28(11), 111901.
- Shahzad, A., F. B. Tian, J. Young and J. C. Lai (2014). Reynolds Number Effects on the Aerodynamic Performance of Wing Planform Shapes in Hover. 19th AFMC, RMIT University, Melbourne, Australia.
- Shahzad, A., F. B. Tian, J. Young and J. C. Lai (2016b). Aerodynamic Hovering Performance of Rigid and Flexible Wing Planform Shapes. *20th Australasian Fluid Mechanics Conference*. Perth, Australia.
- Shahzad, A., F. B. Tian; J. Young and J. C. S. Lai (2017). Numerical study of rigid and flexible wing shapes in hover. *Journal of Physics: Conference Series*, IOP Publishing.
- Shyy, W., H. Aono, C.-K. Kang and H. Liu (2013). *An introduction to flapping wing aerodynamics*, Cambridge University Press, New York, USA.
- Sotavalta, O. (1952). *The essential factor regulating the wing-stroke frequency of insects in wing mutilation and loading experiments and in experiments at subatmospheric pressure*. Suomalainen Eläin- ja Kasvitieteellinen Seura Vanamo, Helsinki, 1-67.
- Tian, F.-B., H. Dai, H. Luo, J. F. Doyle and B. Rousseau (2014a). Fluid-structure interaction involving large deformations: 3D simulations

A. Shahzad *et al.* / *JAFM*, Vol. 12, No. 6, pp. 1979-1988, 2019.

and applications to biological systems. *Journal of computational physics* 258, 451-469.

Weis-Fogh, T. (1973). Quick estimates of flight fitness in hovering animals, including novel mechanisms for lift production. *Journal of Experimental Biology* 59(1), 169-230.

Zhao, L., Q. Huang, X. Deng, S. Sane (2010).

Aerodynamic effects of flexibility in flapping wings. *Journal of The Royal Society Interface* 7(44), 485-497.

Zheng, Y., Y. Wu and H. Tang (2015). Force measurements of flexible tandem wings in hovering and forward flights. *Bioinspiration & biomimetics* 10(1), 1-21.